"OCCURRENCE OF A NEARLY CONSTANT AIR FLUX THROUGH THE ACCUMULATION CHAMBER AND DETERMINATION OF THE TWO COMPONENTS OF THE CO_2 FLUX FROM SOIL. I: LABORATORY EXPERIMENTS "

Ana Hernández-Rodríguez[1,*], Giorgio Virgili[1], Davide Continanza[1], Luca F. Ferrante Vero[1]

[1] West Systems s.r.l., Viale Donato Giannotti 24, Florence, Italy

ABSTRACT

Different types of laboratory experiments were carried out during this study. In type A experiments a standard gas mixture is continuously injected, at constant flux, into the accumulation chamber, mimicking the soil CO_2 flux measurements performed in field surveys. In type B experiments, a standard gas mixture is initially injected into the accumulation chamber for a short lapse of time, to achieve a relatively high CO_2 concentration inside the accumulation chamber; then the injection of the standard gas mixture is stopped and the CO_2 concentration inside the chamber is monitored for a sufficient interval of time. In both types of experiments, the accumulation chamber appears to be flushed by a considerable flux of atmospheric air, which is virtually constant in each experiment but is different from experiment to experiment. The occurrence of this air flux through the accumulation chamber (i) has no effect on the determination of the soil CO_2 flux on the basis of the initial slope (at time zero) of the CO_2 concentration-time curve, but (ii) it complicates the evaluation of the two components of the soil CO_2 flux, namely the CO_2 molar fraction of soil gas and the flux of the soil gas mixture. A method to obtain both the CO_2 molar fraction of soil gas and the flux of the soil gas mixture is presented and the implications related to the knowledge of the two components of the soil CO_2 flux are discussed.

1. INTRODUCTION

Since the early 1990's, the soil CO_2 flux, F_{CO_2}, has been measured, mapped, and monitored at sites worldwide for geothermal exploration, volcanic surveillance, surface monitoring of CO_2 geological sequestration sites and other geo-scientific purposes [e.g., Baubron et al., 1990 1991; Allard et al., 1991; Chiodini et al., 1996, 1998, 2001, 2007, 2008; Hernández et al., 1998, 2001; Carapezza and Federico, 2000; Lewicki and Brantley, 2000; Werner et al., 2000; Bergfeld et al., 2001; Brombach et al, 2001; Salazar et al., 2001; Carapezza and Granieri, 2004; Frondini et al., 2004, 2009; Notsu et al., 2005; Fridriksson et al., 2006; Werner and Cardellini, 2006; Padrón et al., 2008a; Carapezza et al., 2009; Evans et al. 2009; Toutain et al., 2009; Mazot et al.,

2011; Rissmann et al., 2012; Parks et al., 2013; Dionis et al., 2015; Hutchison et al., 2015; Jolie et al., 2015; Lee et al., 2016; Robertson et al., 2016]. Most of these F_{CO_2} studies have been performed adopting the accumulation chamber method, where an inverted chamber is positioned on the ground, the CO_2 concentration inside the chamber is monitored, and the initial slope (at time zero) of the CO_2 concentration-time curve is used to compute the F_{CO_2} [Chiodini et al., 1998].

The method has some limitations and uncertainties. For instance, the F_{CO_2} is affected by changes in atmospheric pressure and other meteorological parameters, such as soil temperature and moisture, wind speed, and rain [e.g., Edwards, 1975; Hanson et al., 1993; Chiodini et al., 1998; Rogie et al., 2001; Salazar et al., 2002; Granieri et al., 2003, 2010; Brusca et al, 2004; Lewicki

et al, 2007; Padrón et al., 2008b; Viveiros et al., 2008, 2009, 2010; Perez et al., 2012; Rinaldi et al., 2012; Lewicki and Hilley, 2014; Padilla et al., 2014; Werner et al., 2014]. Consequently, surveys of F_{CO_2} have to be carried out under dry and stable weather conditions to avoid the detrimental effects caused by variations of meteorological parameters.

Use of the accumulation chamber may change the soil gas flow from its natural undisturbed state by altering the gas pressure inside the chamber, varying the pressure and concentration gradients in the underlying soil, diverting the soil gas flow around the chamber, altering locally soil physical properties (e.g., by inserting a "collar" into the soil to position the chamber), and determining an increase of water vapor within the chamber [Norman et al., 1992; Healy et al., 1996; Evans et al. 2001; Gerlach et al. 2001; Welles et al. 2001]. These effects has been quantified through controlled laboratory tests, showing that measured F_{CO_2} values are 0-25% lower than the imposed F_{CO_2} values, in the range 200 - 12,000 g m^{-2} day^{-1} [Evans et al., 2001]. However, these uncertainties can be mitigated by imposing known F_{CO_2} values and calibrating the system accordingly [Chiodini et al., 1998].

All in all, taking suitable precautions and accepting some minor uncertainties, the accumulation chamber method had been shown to be effective in determining the soil F_{CO_2} values from the low values sustained by decay of organic substances to the high values in areas of steaming ground [Chiodini et al., 1998; Norman et al., 1992, 1997; Lewicki et al., 2005; Lewicki and Hilley, 2014].

In spite of the impressive number of studies carried out in the last 25 years, the potential uses for flux data determined using the accumulation chamber method have not been fully exploited. For instance, the accumulation chamber CO_2 time series can be used, in principle, to obtain not only the F_{CO_2} value but also its two components, namely the molar fraction of CO_2 in the soil gas, $X_{CO_2,G}$, and the flux of the soil gas mixture, FG. Note that only two of the three variables F_{CO_2}, F_G, and $X_{CO_2,G}$ are independent, as they are linked by the simple relation:

$$F_{CO_2} = F_G \cdot X_{CO_2,G} \qquad (1)$$

In addition, the occurrence of gas exchange between the atmosphere and the accumulation chamber needs to be investigated. This paper discusses (1) the results of suitable laboratory experiments aimed at investigating gas exchange between the atmosphere and the accumulation chamber, (2) a method to obtain F_G and $X_{CO_2,G}$

from the CO_2 time series acquired by means of the accumulation chamber method, and (3) the implications related to the knowledge of the two components of F_{CO_2}, in order to underscore why it is important to know not only F_{CO_2} but also F_G and $X_{CO_2,G}$.

2. METHODS

2.1 THE LABORATORY EXPERIMENTS

In this work, all the laboratory experiments were performed using West Systems portable CO_2 fluxmeters comprising the following main components (Figure 1):
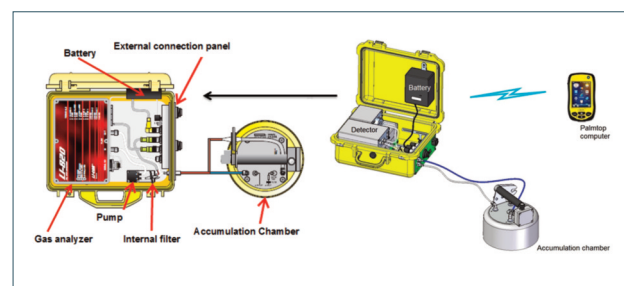
FIGURE 1. The West Systems portable CO_2 flux meter (from the Handbook of the West Systems CO_2 fluxmeter).

(a) A West Systems™ accumulation chamber of type A, equipped with both a 80 rpm fan, to ensure the homogenization of the gas mixture inside the chamber, and a pressure compensation device to maintain pressure equilibrium between inside the chamber and the surrounding air outside the chamber, avoiding the pressurization of the chamber that would alter the gas flow from soil (see above).

(b) A non-dispersive infrared spectrometer as CO_2 analyzer, either a LICOR LI-820™ or a Vaisala CARBOCAP® CO_2 sensor GMP343. The CO_2 analyzer performs the continuous determination of CO_2 concentration inside the accumulation chamber. The main technical specifications of the LICOR LI-820™ are: measurement range 0-20,000 ppmv; root mean square noise <1 ppmv at 370 ppmv with 1 s signal filtering; accuracy 3% of reading. The main technical specifications of the Vaisala GMP343™ are: measurement range 0-20,000 ppmv; noise at 370 ppm CO_2 ± 3 ppmv CO_2; accuracy ± (5 ppmv + 2% of reading).

(c) A membrane pump that provides continuous transfer of the gas from the accumulation chamber to the CO_2 analyzer and back into the chamber through the inlet and outlet tubes. The

fluxmeters were equipped with one of the following three pumps KNF NMP830, KNF NF30, and KNF NMS020. The flowrate of each pump was measured with an accuracy close to 1% by using a Gilian Gilibrator-2 NIOSH Primary Standard Air Flow Calibrator, obtaining the following values: 47.5 cm^3 s^{-1} for KNF NMP830, 35.5 cm^3 s^{-1} for KNF NF30, and 24.2 cm^3 s^{-1} for KNF NMS020.

(d) A palmtop computer for data acquisition with the frequency of one record per second. Acquired data include: time, CO$_2$ concentration, pressure and temperature in the measuring cell of the CO$_2$ analyzer, ambient temperature and barometric pressure. Cell pressure and barometric pressure are recorded only by the fluxmeter equipped with the LICOR LI-820™ CO$_2$ analyzer.

Further details are given by the handbook of the West Systems CO$_2$ fluxmeter (https://www.westsystems.com/wp-content/uploads/2018/01/Handbook_Portable_8.2.pdf). The fluxmeter comprising the accumulation chamber, the inlet and outlet tubes, the cell of the CO$_2$ analyzer and filters has a net total volume of 3063 cm3, whereas the accumulation chamber has a basal area of 314 cm^2.

In the adopted experimental set up (Figure 2a), the accumulation chamber is positioned with the opening on a desk, either inserting a rubber gasket over its rim (Figure 2b), to minimize the possible input of atmospheric air (see below), or without a gasket. The desk surface is impermeable to air and is equipped with a gas injection point which conveys the standard gas mixture, at the selected flux, from the cylinder to the accumulation chamber.

The gas flux is controlled by using an electronically stabilized mass flow controller [Alicat Scientific MC-2LPM-D™] with a full scale accuracy $\pm$ 0.2%, a working range from 0.17 to 33.33 cm^3 s^{-1} and repeatability of $\pm$ 0.2 %. The used gas mixtures have the following compositions (percentages by volume): (a) 2 % CO$_2$, 1% CH$_4$, 97% N$_2$; (b) 9 % CO$_2$, 91% N$_2$ and (c) 50 % CO$_2$, 50 % CH$_4$.

Three types of experiments were performed, called A, B, and C. In type A experiments, the standard gas mixture is continuously injected into the accumulation chamber keeping the gas flux constant at the selected value. These experiments mimic the F_{CO_2} measurements performed in field surveys.

In type B experiments: (1) the standard gas mixture is injected into the accumulation chamber for a short in-
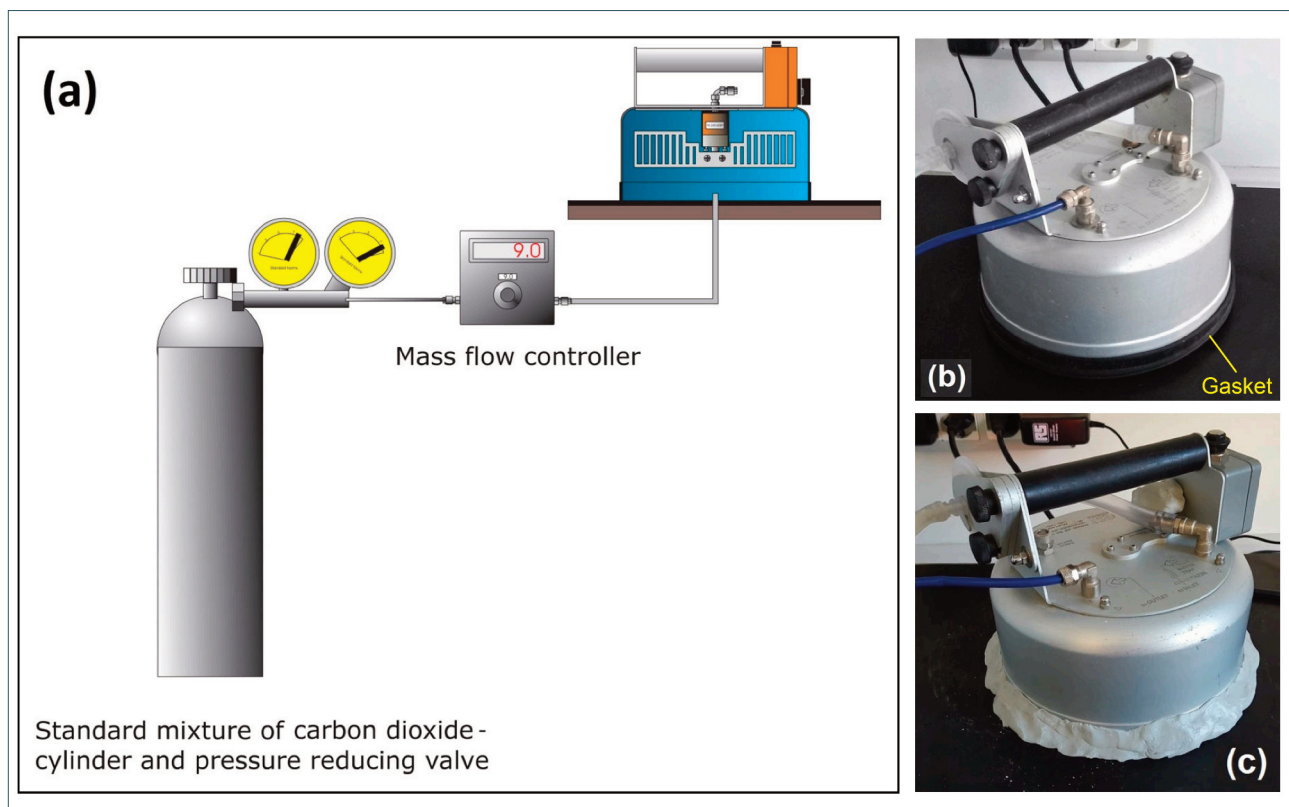
FIGURE 2. (a) Experimental set up adopted in the West Systems laboratory (from the Handbook of the West Systems CO$_2$ fluxmeter, modified). Note that the accumulation chamber is positioned on the desk over the gas injection point either with the rubber gasket or without it. (b) Accumulation chamber with the rubber gasket in the type B experiments. (c) Accumulation chamber during the experiments of type C, in which plaster was used to seal both the chamber - desk interface and the pressure compensation device.

terval of time, typically 100-120 s, to achieve a CO_2 concentration inside the accumulation chamber of ~7000 ppmv; (2) the gas injection is stopped, and the fluxmeter continues to operate to monitor the CO_2 concentration inside the chamber for an interval of time, typically 1900-2100 s. These experiments are used to understand if the accumulation chamber is flushed or not by atmospheric air and to quantify the air flux if any.

The type C experiments are similar to those of type B. The only difference is the use of plaster to seal both the chamber - desk interface and the pressure compensation device (Figure 2c). These experiments are utilized to verify the absence of gas leaks.

The three different standards were used in the three different types of experiments but no difference in behavior was observed when different standards were used.

2.2 METHODS OF INTERPRETATION OF CO_2 TIME SERIES

To interpret the CO_2 time series acquired during the laboratory experiments the system is modeled as a perfectly-mixed single box. Two distinct mass balances can be written as detailed below. In this communication, simple mass balances involving the total soil-chamber-atmosphere CO_2 mass exchanges are preferred to equations in which the diffusive and advective components of the soil gas flux are considered separately [e.g., Welles et al., 2001] due to the ambiguities in the characterization and separation of these two distinct components.

Approach (1) is based on the hypothesis that the accumulation chamber is not flushed by atmospheric air. It means that the flux of the standard gas mixture entering the accumulation chamber is balanced, at any time, by the flux of gas mixture leaving it through either the space between the chamber rim and the desk or the pressure compensation device or both. This hypothesis was adopted by Chiodini et al. [1998].

Approach (2) is based on the assumption that the gas mixture leaving the accumulation chamber comprises the standard gas mixture plus a flux of atmospheric air. In other terms, the accumulation chamber is considered to be flushed by a continuous flux of the standard gas mixture and a continuous flux of atmospheric air. The need to invoke approach (2) will become apparent in the following discussion.

2.2.1 METHODS OF INTERPRETATION OF CO_2 TIME SERIES: APPROACH (1)

The CO_2 time series for approach (1) is described by the following Equation [e.g., Leib et al., 2008]:

$$X_{CO_2,t+dt} \cdot V = X_{CO_2,t} \cdot V + X_{CO_2,G} \cdot F_G \cdot dt - X_{CO_2,t} \cdot F_{out} \cdot dt \quad (2)$$

where: t (s) stands for time, V (cm^3) is the volume of the flux meter comprising the accumulation chamber, the inlet and outlet tubes, the cell of the CO_2 analyzer and filters, $X_{CO_2,t+dt}$ and $X_{CO_2,t}$ (mol/mol) designate the CO_2 molar fraction in the accumulation chamber at time $t+dt$ and at time t, respectively, $X_{CO_2,G}$ (mol/mol) represents the CO_2 molar fraction of the standard gas mixture, F_G and F_{out} (cm^3 s^{-1}) stand for the flow rates of the standard gas mixture entering and leaving the accumulation chamber, respectively, which are assumed to be equal to each other, that is:

$$F_G = F_{out}. \quad (3)$$

Dividing both sides of Equation (2) by V and considering that $X_{CO_2,t+dt} - X_{CO_2,t} = dX_{CO_2}$, Equation (2) can be rearranged as follows:

$$\frac{dX_{CO_2}}{dt} = \frac{F_G \cdot X_{CO_2,G}}{V} - \frac{F_G}{V} X_{CO_2,t} \quad (4)$$

Note that in the plot of dX_{CO_2} vs. X_{CO_2}, Equation (4) defines a straight line of slope $-F_G/V$ and intercept $F_G \cdot X_{CO_2}/V$.

2.2.2 METHODS OF INTERPRETATION OF CO_2 TIME SERIES: APPROACH (2)

To take air inputs into consideration, Equation (2) has to be modified as follows:

$$X_{CO_2,t} = \frac{F_G \cdot X_{CO_2,G} + F_A \cdot X_{CO_2,A}}{F_G + F_A} + k \cdot \exp\left(-\frac{F_G + F_A}{V} \cdot t\right) \quad (5)$$

where $X_{CO_2,A}$ (mol/mol) represents the CO_2 molar fraction of atmospheric air, F_A (cm^3 s^{-1}) is the flow rate of atmospheric air entering the accumulation chamber.

Equation (5) assumes that, at any time, the sum of the standard gas mixture flux and atmospheric air flux is equal to gas flux leaving the accumulation chamber. Again, dividing both sides of Equation (5) by V and considering that $X_{CO_2,t+dt} - X_{CO_2,t} = dX_{CO_2}$, it can be rewritten as follows:

$$\frac{dX_{CO_2}}{dt} = \frac{F_G \cdot X_{CO_2,G} + F_A \cdot X_{CO_2,A}}{V} - \frac{F_G + F_A}{V} X_{CO_2,t} \quad (6)$$

In the plot of dX_{CO_2}/dt vs. X_{CO_2}, Equation (6) defines a straight line of slope $-(F_G+F_A)/V$ and intercept $(F_G \cdot X_{CO_2,G} + F_A \cdot X_{CO_2,A})/V$. Equation (6) is a first order

---

[1] NOTE THAT EQUATION (2) CORRESPONDS TO EQUATION (3) OF CHIODINI ET AL. [1998], ALTHOUGH CO_2 FLUXES ARE EXPRESSED IN CM3 S-1 IN THIS WORK AND IN CM^3 S^{-1} CM^{-2} (OR CM S^{-1}) IN CHIODINI ET AL. [1998]. THE CONVERSION FACTOR IS THE BASAL AREA OF THE ACCUMULATION CHAMBER, 314 CM^2. THE CM^3 S^{-1}WAS ADOPTED AS MEASUREMENT UNIT OF THE GAS FLOW BECAUSE THE SECTION RELATED TO THE FLUX OF ATMOSPHERIC AIR FLUSHING THE SYSTEM IS UNKNOWN (SEE BELOW).

linear ordinary differential Equation, whose general solution is:

$$X_{CO_2,t} = \frac{F_G \cdot X_{CO_2,G} + F_A \cdot X_{CO_2,A}}{F_G + F_A} + k \cdot \exp\left(-\frac{F_G + F_A}{V} \cdot t\right) \quad (7)$$

where k is a constant. To find k, t is set equal to zero, obtaining:

$$k = X_{CO_2,0} - \frac{F_G \cdot X_{CO_2,G} + F_A \cdot X_{CO_2,A}}{F_G + F_A} \quad (8)$$

where $X_{CO_2,0}$ is the initial value of the CO$_2$ molar fraction inside the accumulation chamber. Hence, Equation (7) can be rewritten as follows:

$$X_{CO_2,t} = \frac{F_G \cdot X_{CO_2,G} + F_A \cdot X_{CO_2,A}}{F_G + F_A} +$$

$$\left(X_{CO_2,0} - \frac{F_G \cdot X_{CO_2,G} + F_A \cdot X_{CO_2,A}}{F_G + F_A}\right) \quad (9)$$

$$\cdot \exp\left(-\frac{F_G + F_A}{V} \cdot t\right)$$

Equation (9) represents the theoretical basis for the method used in section 4.1 to obtain F_G and $X_{CO_2,G}$ from the accumulation chamber CO$_2$ time series.

3. RESULTS

3.1 THE TYPE C EXPERIMENTS

For all the type C experiments, the CO$_2$ concentration-time curve includes:

(1) a quick build up determined by the rate of CO$_2$ input into the accumulation chamber, followed by

(2) flattening of the curve due to the almost constant CO$_2$ content after ending the CO$_2$ input into the accumulation chamber (Figure 3).

Since plaster is not totally impermeable to gases, the CO$_2$ concentration-time curve deviates from the ideal of constant CO$_2$ content. The decrease in CO$_2$ concentration with time, although very small, depends on the flowrate of the membrane pumps, F_P, with values of

(a) -1.1 · 10^{-7} to -2.6 · 10^{-7} s^{-1} for runs 2 and 4, for a membrane pump flowrate of 24.2 cm^3 s^{-1}, and

(b) -3.4 · 10^{-7} to -5.0 · 10^{-7} s^{-1} for runs 1 and 3, for a pump flowrate of 47.5 cm^3 s^{-1}.

The average difference between the atmospheric pressure and the pressure in the cell of the LICOR LI-820™ CO$_2$ analyzer, ΔP^*, was 43.4 mbar in run 1, 19.2 mbar in run 2, 43.9 mbar in run 3 and 18.9 mbar in run 4.
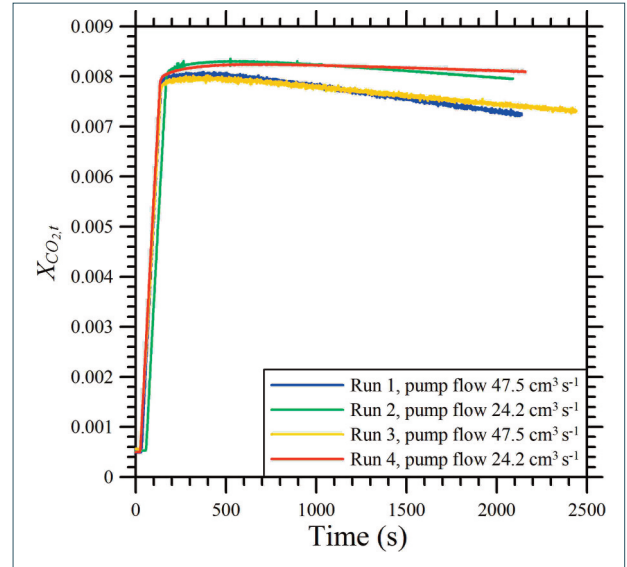
FIGURE 3. Plot of the measured CO$_2$ concentration inside the accumulation chamber versus time for four experiments of type C, in which plaster was used to seal both the chamber - desk interface and the pressure compensation device.

3.2 THE TYPE B EXPERIMENTS

The CO$_2$ concentration-time curve for all type B experiments comprises a fast build up caused by the injection of CO$_2$, followed by a relatively slow drawdown, upon cessation of the CO$_2$ injection into the accumulation chamber (Figure 4). The CO$_2$ injection was performed at flowrates similar to those adopted in type C experiments. The buildup curve does not give any information of interest. In contrast, the form of the drawdown curve, with decrease of CO$_2$ concentration with time and negative slope also decreasing with time, indicates that the accumulation chamber is continuously flushed by atmospheric air. In fact, in the absence of such atmospheric air flush, the CO$_2$ concentration inside the accumulation chamber would be expected to remain constant or nearly so at the maximum value achieved due to CO$_2$ injection into the chamber, as it is observed in the experiments of type C (see section 3.1).

In addition to this important qualitative information on the gas exchanges between the atmosphere and the accumulation chamber, the drawdown curve was used to determine by trial and error the flux of atmospheric air flushing the chamber assuming that it is constant. The sought solution corresponds to the minimum of the average absolute deviation (AAD) between measured $X_{CO_2,t}$ values and calculated $X_{CO_2,t}$ values from Equation (5).

Both the measured CO$_2$ concentrations and the corresponding calculated CO$_2$ values are plotted against time for the two experimental runs of type B 152131 and 161126 in Figure 4. Run 152131 (Figure 4a) utilized a
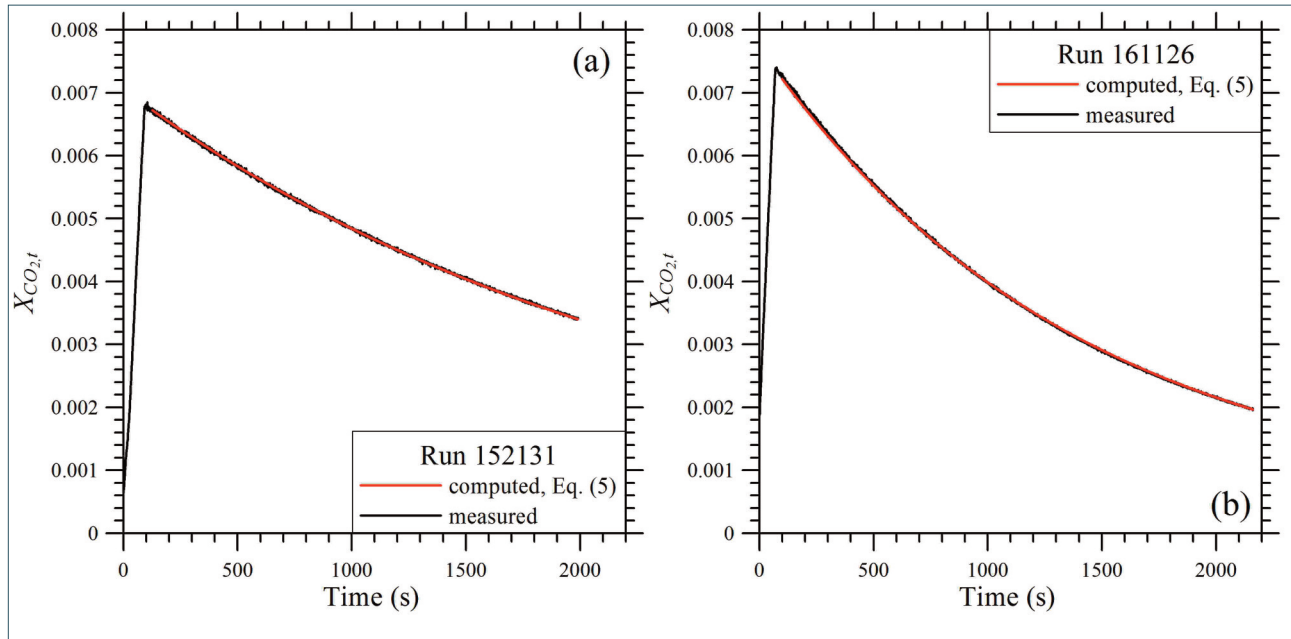
FIGURE 4. Plot of the measured and computed CO_2 concentration inside the accumulation chamber versus time for two experimental runs of type B 152131 and 161126. Run 152131 (a) was performed inserting a rubber gasket over the rim of the accumulation chamber whereas run 161126 (b) was carried out placing the accumulation chamber directly on the desk over the gas injection point without any gasket.

rubber gasket placed over the rim of the accumulation chamber, whereas there was no gasket for run 161126 (Figure 4b) where the accumulation chamber was placed over the gas injection point and sat directly on the desk. For both runs there is a perfect match between the measured drawdown curve and the calculated counterpart, with an AAD of 0.26% and a maximum absolute deviation (MAD) of 1.2% in the run with the rubber gasket and with an AAD of 0.38% and a MAD of 1.5%, in the run without the gasket. The main results of the experimental runs of type B, including those depicted in Figure 4, are reported in Table 1, showing that there is a very good correspondence between the measured drawdown curves and the calculated counterparts, with AAD values of 0.14 to 1.54%. Since the $X_{CO_2,t}$ values computed using Equation (5) reproduce with acceptable accuracy the corresponding measured $X_{CO_2,t}$ values, the starting hypothesis is satisfied, i.e., the flux of atmospheric air flushing the accumulation chamber during the experiments of type B can be considered to be virtually constant.

Table 1 also shows that F_A represents 1.4 to 2.8 % of F_P in the experiments with the rubber gasket, whereas F_A constitutes 2.2 to 4.7 % of F_P in most experimental runs without the gasket, apart from run 144401, with F_A equal to 1.4% of F_P, and run 122850, with F_A equal to 6.6% of F_P. The lower F_A/F_P ratios of the experiments with the rubber gasket are not surprising since the gas-

ket acts as a partial seal and reduces the flow of air entering the accumulation chamber.

3.3 THE XCO$_2$ - TIME CURVE OF TYPE A EXPERIMENTS

Plots of CO_2 concentration versus time are shown in Figure 5 for four selected type A experiments, 103212, 154723, 112311, and 141306, all with F_G in the range 1.67 to 6.67 cm^3 s^{-1}.

In these plots, the measured CO_2 time series (black line) are compared with the corresponding CO_2 time series calculated using: (i) Equation (2), i.e., assuming that the accumulation chamber is not flushed by atmospheric air (blue curve) and (ii) Equation (5), i.e., assuming that the accumulation chamber is flushed by a constant flux of atmospheric air (red curve). Again, since the flux of atmospheric air through the chamber is unknown, it was obtained by trial and error until the AAD between measured and computed data attains the minimum value.

These CO_2-time plots show that results calculated using Equation (2) overestimate significantly the measured CO_2 time series, whereas results computed using Equation (5) closely approximate the measured CO_2 time series. Note that the agreement between the measured and calculated results for a constant flux of atmospheric air are very good for the three type A experiments 103212, 154723, and 112311, of duration ranging between ~600

Code	ΔP^* mbar	F_P cm^3 s^{-1}	F_A cm^3 s^{-1}	Gasket	Duration s	AAD %	$100 \cdot (F_A / F_P)$ %
152131	45.7	47.5	1.310	Yes	1991	0.26	2.8
105250	–	47.5	0.768	Yes	2369	0.75	1.6
115215	–	24.2	0.381	Yes	2064	0.30	1.6
145200	–	47.5	1.030	Yes	2508	0.69	2.2
153741	–	24.2	0.581	Yes	2355	0.65	2.4
95957	33.5	35.5	0.482	Yes	2623	0.14	1.4
113154	33.5	35.5	0.958	Yes	2247	0.99	2.7
140400	33.6	35.5	0.982	Yes	2278	0.80	2.8
161126	46.4	47.5	2.210	No	2161	0.38	4.7
122850	–	47.5	3.130	No	2352	1.54	6.6
141406	–	24.2	0.789	No	2173	0.49	3.3
164527	–	47.5	1.270	No	2832	1.12	2.7
173700	–	24.2	1.010	No	1518	0.78	4.2
105130	33.9	35.5	0.927	No	2249	1.15	2.6
121233	33.6	35.5	0.789	No	2106	1.07	2.2
144401	33.9	35.5	0.513	No	2333	0.78	1.4

TABLE 1. Main characteristics of some experimental runs of type B. The experiments with code in bold are displayed in Figure 4. ΔP^* is the average difference between the atmospheric pressure and the pressure in the cell of the LICOR LI-820™ CO_2 analyzer. These data are not available for the Vaisala CARBOCAP® CO_2 analyzer.

Code	X_{CO_2}	F_G cm^3 s^{-1}	F_A cm^3 s^{-1}	Gasket	Duration s	AAD %	$F_A / (F_A + F_G)$
103212	0.09	1.67	2.26	Yes	590	0.84	0.58
141142	0.09	1.67	2.20	No	560	1.54	0.57
112311	0.02	1.67	1.77	Yes	1809	0.64	0.52
104636	0.09	1.67	2.54	Yes	714	2.37	0.60
141306	0.02	1.67	0.354	Yes	7049	2.69	0.18
113108	0.02	3.33	1.25	No	1481	2.14	0.27
154723	0.02	5.00	1.05	No	822	1.09	0.17
155254	0.09	5.00	1.00	No	160	1.82	0.17
121322	0.02	6.67	0.550	Yes	1982	3.37	0.08

TABLE 2. Main characteristics of some experimental runs of type A with F_G of 1.67-6.67 cm^3 s^{-1}. The experiments with code in bold are displayed in Figure 5.

and ~1800 s (Figure 5a, b, and c, respectively). In contrast, the agreement for type A experiment 141306, with a much longer duration, ~7000 s is less satisfactory (Figure 5d). Results show a crossover between the measured data curve and the computed curve (for a constant flux of atmospheric air) that might be due to the moderate decrease of the atmospheric air flux with time, an effect which is evidently detectable only in experiments of long duration at these F_G values.

The main characteristics of some experimental runs of type A, with F_G in the range 1.67 to 6.67 cm^3 s^{-1}, including those displayed in Figure 5, are reported in Table 2, showing that:
(i) the AAD between measured and computed data is low, varying between 0.64 and 3.37%;
(ii) F_A decrease progressively with increasing F_G (Figure 6), apart from the long-duration experiment 141306, and
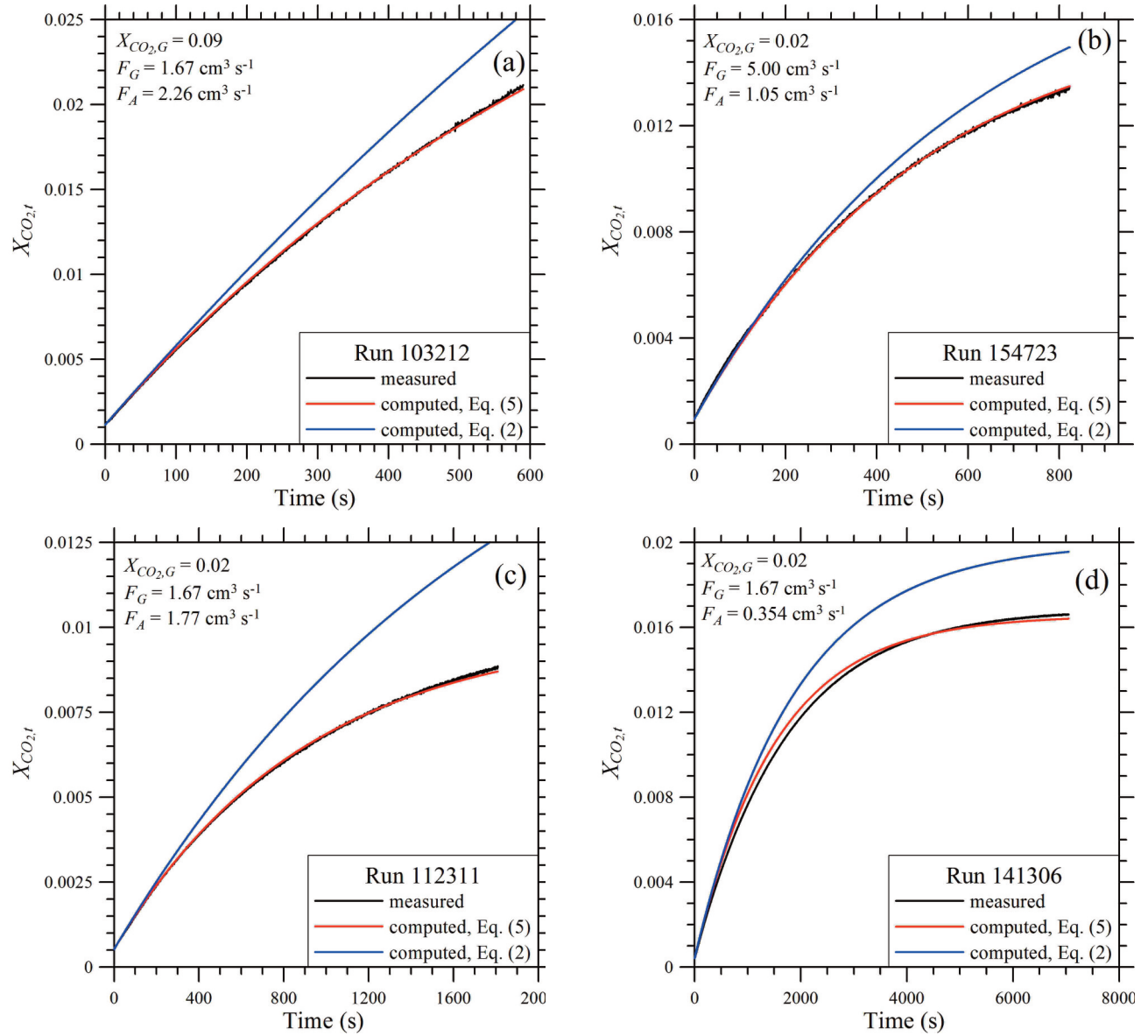
FIGURE 5. Plot of CO_2 concentration in the accumulation chamber versus time for four selected experiments of type A showing the measured CO_2 time series (black line), the CO_2 time series calculated using Equation (2), i.e., assuming that the accumulation chamber is not flushed by atmospheric air (blue curve), and the CO_2 time series calculated using Equation (5), i.e., assuming that the accumulation chamber is flushed by a constant flux of atmospheric air (red curve).

(iii) consequently, the $F_A/(F_A+F_G)$ ratio decreases gradually from 0.52-0.60 at F_G of 1.67 cm^3 s^{-1} to 0.08 at F_G of 6.67 cm^3 s^{-1}.

Type A experiments with F_G in the range 0.0833 to 0.833 cm^3 s^{-1}:

(i) have higher AAD between measured and computed data,

(ii) exhibit a crossover between the measured data line and the computed curve,

(iii) have high F_A values, in the range 5 to 10 cm^3 s^{-1}, and

(iv) have, therefore, high $F_A/(F_A+F_G)$ ratios, from 0.85 to 0.99. Since the results for the type A experi-

ments with F_G in the range 0.0833 to 0.833 cm^3 s^{-1} are affected by relatively high uncertainties, whose origins are not properly understood, they are not considered in the following discussion.

4. DISCUSSION

The accumulation chamber was flushed by atmospheric air in all the laboratory experiments of type A and B. F_A is virtually constant in each type B experiment as well as in each type A experiment of duration lower than 1800-2000 s, but F_A is different from experiment to experiment.
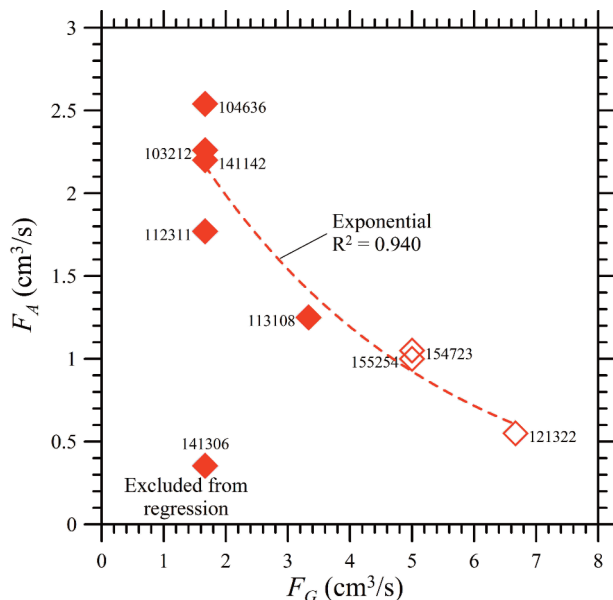
FIGURE 6. Plot of F_A vs. F_G for some experiments of type A, with F_G in the range 1.67 to 6.67 cm3 s-1. The exponential model was adopted to fit the F_A and F_G-values since the squared regression coefficients is higher than for other models. Closed symbols identify experiments with the gasket whereas open symbols refer to experiments without the gasket.

FIGURE 7. Plot of $\Delta P^* = P_{atm} - P_{cell}$ vs. the membrane pump flowrate, F_P for the experiments of type B, with the rubber gasket and without it, and type C (see legend)..

The occurrence of this considerable air flux through the chamber raises some questions, the first and most important is **does the air flux affect the determination of F_{CO_2}?** To answer this question, it must be noted that Equation (6), which incorporates the air flux through the chamber, reduces to;

$$F_{CO_2} = \frac{dX_{CO_2}}{dt} \cdot V \tag{10}$$

at the initial conditions, i.e., at time zero. Equation (10) corresponds to Equation (7) of Chiodini et al. [1998] which is used to evaluate F_{CO_2} on the basis of the initial slope (at time zero) of the CO_2 concentration-time curve. The only difference between these two Equations is the physical dimension (and consequently the measurement unit) of F_{CO_2}, which is [volume · time⁻¹ · area⁻¹] in Chiodini et al. [1998] and [volume · time⁻¹] in this work. Leaving aside this difference, the important thing to be noted is that F_A does not appear in Equation (10) and, therefore, the flux of air through the accumulation chamber has no effect on the determination of the F_{CO_2}.

A second question is **what are the entry and exit points through which air enters and leaves the chamber?** Before answering this question it must be recalled that maintenance of pressure equilibrium between inside the chamber and the surrounding air outside the chamber is a necessary requirement so that the measured F_{CO_2} and its two component terms (F_G and $X_{CO_2,G}$) can

be truly representative of the natural values [e.g., Xu et al., 2006]. For this reason, the chamber is equipped with a pressure compensation device. For the same reason, an effective seal cannot be emplaced between the chamber and either the soil surface in field deployment or the desk surface in laboratory tests **(2)**. Only a gasket can be used to minimize the inflow of atmospheric air during the measurements, as done in some experiments of type A and B (see above). Therefore, it can be assumed that atmospheric air may enter and leave the accumulation chamber through both the interface between the chamber rim and the surface onto which the chamber rests and the pressure compensation device. The second pathway is considered less likely unless the pressure inside the chamber, P_{AC}, attains a value significantly higher than the external atmospheric pressure, P_{atm}.

The data obtained during the experiments of type B and C carried out using the LICOR infrared spectrometer can be used to evaluate the difference $\Delta P = P_{atm} - P_{AC}$, since both P_{atm} and the pressure in the measuring cell of the LICOR CO_2 analyzer, Pcell, are continuously recorded during these runs. As noted earlier, pressure data are not available for the experiments performed using the Vaisala CARBOCAP CO_2 analyzer. Hence, the difference $\Delta P^* = P_{atm} - P_{cell}$ can be computed. ΔP^* can be considered a proxy of ΔP assuming that P_{cell} is similar to P_{AC}. Since the oscillations of ΔP^* during the experi

---

ments are in the order of ~1 mbar, ΔP^* data were averaged and reported in Table 1 for the experiments of type B and in section 3.1 for the experiments of type C. The results show the average ΔP^* results are strongly dependent on F_P (Figure 7) as described by the following linear regression Equation (ΔP^* in mbar, F_P in cm³ s⁻¹, N = 12, R^2 = 0.963):

$$\Delta P^* = 0.936 \cdot F_P. \qquad (11)$$

The dependence of ΔP^* on F_P suggests that the pumping rate controls the pressure distribution in the measuring systems during the experiments of types B and C.

A third question is **what controls F_A?** To answer this question let us consider the plot of F_A vs. F_P for the type B experiments (Figure 8) for the time after the gas flow is turned off and the only flow is driven by the membrane pump circulating gas from the accumulation chamber to the CO_2 analyzer and back.

Figure 8 shows that the spread of points is limited for the type B experiments with the rubber gasket, whose F_A and F_P data fit the following linear regression Equation through the origin (R = 0.722):

$$F_A = 0.0219 \cdot F_P. \qquad (12).$$

The R value, 0.722, is significant at probability < 5% for N-2 = 6 degrees of freedom, suggesting that the relation between F_A and F_P is statistically meaningful. In contrast, the type B experiments without the gasket
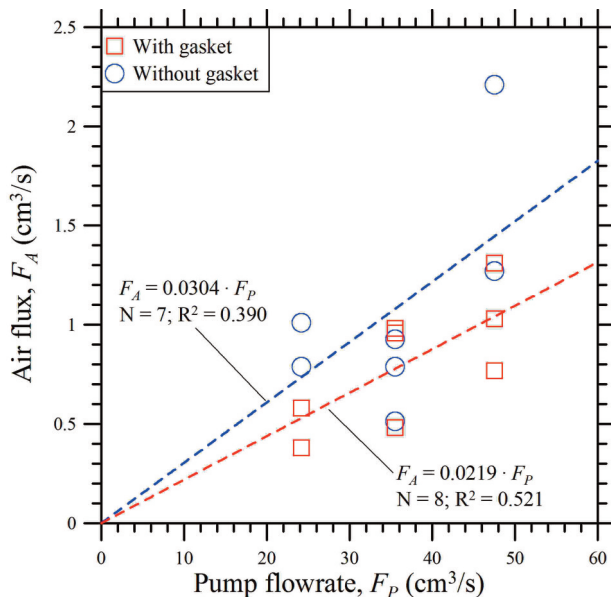
FIGURE 8. Plot of the air flux, F_A, vs. the membrane pump flowrate, F_P for the experiments of type B with the rubber gasket and without it (see legend). Experiment 122850 is not plotted due to its high F_A, 3.13 cm³ s⁻¹, and its high AAD, 1.54% (Table 1).

show a remarkable spread of points, also considering that experiment 122850 is not plotted in Figure 8 due to the high F_A, 3.13 cm³ s⁻¹, and the high AAD, 1.54% (Table 1). The F_A and F_P values for the type B experiments without the gasket fit the following linear regression Equation through the origin (R = 0.622)

$$F_A = 0.0304 \cdot F_P \qquad (13)$$

The R value, 0.622, is not significant at 10% of probability for N-2 = 5 degrees of freedom, suggesting that the relation between F_A and F_P is statistically meaningless.

Equation (12) has a slope lower than that of Equation (13) since as noted above, the rubber gasket acts to some extent as a seal, reducing the flux of air through the chamber. The poor relation between F_A and F_P for the type B experiments without the gasket is probably due to the variable size of the cross-sectional area available for air flow, reflecting the irregularities of the desk surface onto which the chamber is positioned from one experiment to another. In contrast, use of the rubber gasket seems to decrease the variability of the cross-sectional area to air flow. Irrespective of the somewhat erratic results of the experimental runs without the gasket, there is no doubt that the membrane pump flowrate, F_P controls the air flux, F_A, in all the type B experiments.

In type A experiments with F_G in the range 1.67 to 6.67 cm³ s⁻¹ and with durations lower than 1800-2000 s, F_A appears to be strictly related to F_G as shown in Figure 6. It must be noted that in type A experiments there is both a gas flow entering the chamber from below and a gas flow driven by the membrane pump. Consequently, the gas exchanges between the chamber and the atmosphere are probably more complex than in the experiments of type B. In spite of these complexities, for type A experiments F_A is neither a random effect nor a noise, but it is due to the unavoidable gas exchange between the chamber and the atmosphere. This gas exchange must be taken into account in order to use the measured CO_2 time series to estimate F_G and $X_{CO_2,G}$.

4.1 A METHOD TO OBTAIN F_G AND $XCO_{2,G}$

To obtain the two components of the soil CO_2 flux, the accumulation chamber CO_2 concentration data are fitted against time adopting Equation (9) as theoretical model, treating F_G, $X_{CO_2,G}$, and F_A as adjustable coefficients, and assuming that $X_{CO_2,A}$ is equal to $X_{CO_2,0}$ (3). The results of some type A experiments are used to test this method by comparing the known F_G, $X_{CO_2,G}$, and F_{CO_2} values with the corresponding computed values.

Run	F_G (cm^3 s^{-1})			$X_{CO_2,G}$			F_{CO_2} (cm^3 s^{-1})			F_A (cm^3 s^{-1})		
	Known	Comp.	%dev.	Known	Comp.	%dev	Known	Comp.	%dev	Section 3.3	Section 4.1	%dev
103212	1.67	1.61	-3.3	0.09	0.0877	-2.6	0.150	0.142	-5.8	2.26	1.93	-7.20
104636	1.67	1.60	-4.2	0.09	0.0875	-2.8	0.150	0.140	-6.9	2.54	1.82	-14.27
141142	1.67	1.69	1.4	0.09	0.0907	0.8	0.150	0.153	2.1	2.20	2.84	14.44
155254	5.00	5.00	-0.1	0.09	0.0899	-0.1	0.450	0.449	-0.2	1.00	1.47	23.44
112311	1.67	1.59	-4.9	0.02	0.0194	-2.8	0.033	0.031	-7.6	1.77	1.69	-2.23
141306	1.67	1.49	-10.7	0.02	0.0198	-1.1	0.033	0.030	-11.7	0.35	0.30	-6.98
113108	3.33	3.40	2.0	0.02	0.0197	-1.4	0.067	0.067	0.6	1.25	1.75	19.20
154723	5.00	4.92	-1.7	0.02	0.0198	-1.2	0.100	0.097	-2.9	1.05	1.26	9.84
121322	6.67	5.72	-14.2	0.02	0.0199	-0.5	0.133	0.114	-14.7	0.55	0.40	-13.72

TABLE 3. Known and computed F_G, $X_{CO_2,G}$, and F_{CO_2} values for some experimental runs of type A. The F_A values computed by means of the method discussed in this section and that of section 3.3 are also listed..

Table 3 shows those results and two sets of F_A values, obtained through use of Equation 9, described in this section and Equation 5, outlined in section 3.3. Also listed in Table 3 is the percent deviation, %dev, which is calculated with respect to the known value for F_G, $X_{CO_2,G}$, and F_{CO_2} and using the average of the two computed values for F_A because the true value is unknown. The average of the absolute values of %dev, is 4.7% for F_G, 1.5% $X_{CO_2,G}$, 5.8% for F_{CO_2}, and 12.4% for F_A. Based on these data, it can be concluded that the adopted method reproduces F_G, $X_{CO_2,G}$, and F_{CO_2} with acceptable approximations. The larger uncertainties on F_A derive from the two distinct approaches adopted to compute the two F_A series. In any case, the uncertainties on F_A determine related uncertainties on F_G and $X_{CO_2,G}$ but do not affect the validity of the method proposed here to obtain the two components of the soil CO$_2$ flux. The use of this method in the field requires further tests representing the subject of a separate communication.

4.2 IMPLICATIONS

There are at least two important implications that come from having knowledge of F_G, and $X_{CO_2,G}$, the two components of F_{CO_2}. Through the use of bivariate statistics and geostatistics on these data our understanding of the natural systems of interest can be improved to a significant extent. For instance, it should be possible to understand if high F_{CO_2} values are controlled by (i) high F_G values, (ii) high $X_{CO_2,G}$ values, or (iii) high values of both variables and, conversely, if low F_{CO_2} values are due to either (a) low F_G values, (b) low $X_{CO_2,G}$, or (c) low values of both parameters.

The other implication is the proper interpretation of

isotopic data, which has been the subject of several recent papers [e.g., Chiodini et al., 2008; Parks et al., 2013; Lee et al., 2016; Robertson et al., 2016; Hutchison et al., 2016]. To discuss this point, let us assume that two gas samples are collected from the accumulation chamber, as was done by Chiodini et al. [2008]. The first sample (sample A) is collected after a few seconds to allow homogenisation of the gas mixture inside the chamber, whereas the second sample (sample B) is collected some time later, at higher CO$_2$ concentration. Both samples are then analyzed for the δ^{13}C$_{CO_2}$ value. The X_{CO_2} and δ^{13}C$_{CO_2}$ value of the two samples constrain the mixing line between pure soil gas and air, which is a straight line in the plot of δ^{13}C$_{CO_2}$ vs. the inverse of X_{CO_2} [Faure, 1986], as schematically shown in Figure 9.

This plot also shows that it is possible to reconstruct the δ^{13}C$_{CO_2}$ value of soil gas, δ^{13}C$_{CO_2,G}$, by reading the δ^{13}C$_{CO_2}$ value corresponding to X_{CO_2} along the mixing line between pure soil gas and air. This is why knowing the CO$_2$ concentration of soil gas is of utmost importance for the proper interpretation of the δ^{13}C$_{CO_2}$ values of soil gas – air mixtures collected inside the accumulation chamber. Alternatively, one can wait until the gas inside the accumulation chamber is presumably constituted by pure soil gas or almost so and sample it to obtain a representative δ^{13}C$_{CO_2}$ value. However, this might be a tedious, very long procedure and, moreover, it is difficult to check if the gas inside the accumulation chamber is actually representative of soil gas or not without knowing X_{CO_2}.

Of course this discussion only applies for studies when gas samples for chemical and isotopic analyses of CO$_2$ are collected from the accumulation chamber, and isn't needed when soil gases are sampled using a probe to penetrate the soil to a suitable depth [e.g., Salazar et al., 2001; Federico et al., 2010; Dionis et al., 2015].

[3] ALTERNATIVELY, ASSUMING A CONCENTRATION OF 400 PPMV FOR AIR (THE PRESENT ATMOSPHERIC VALUE) LEADS TO NEGLIGIBLE CHANGES IN CALCULATION RESULTS.
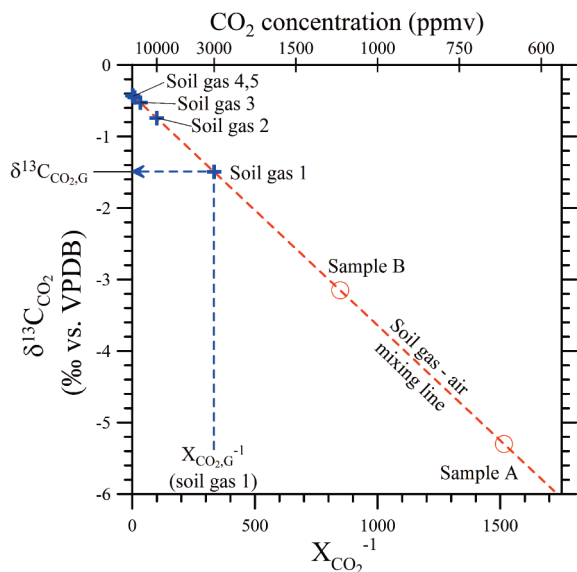
FIGURE 9. Plot of the d^{13}C value of CO_2 vs. the inverse of the CO_2 molar fraction for two soil gas – air mixtures collected inside the accumulation chamber, samples A and B, which constrain the soil gas – air mixing line (red dashed line). The inverse of the CO_2 molar fraction of soil gas (Soil gas 1) allows one to estimate the ^{13}C value of CO_2 of soil gas, following the blue dashed line with arrow. Other soil gas compositions (Soil gas 2, 3, 4, and 5) are used to discuss the error on the computed d^{13}C value of CO_2 based on the assumption that soil gas is constituted by pure CO_2 (see text).

5. CONCLUSIONS

Three distinct types of laboratory experiments were performed to investigate gas exchanges between the atmosphere and the accumulation chamber and to implement a method to obtain F_G and $X_{CO_2,G}$, from CO_2 time series data.

The results from the experiments show a considerable air flux through the chamber that is practically constant in each run but differs from run to run.

It seems likely that the interface between the chamber rim and the surface represents the main entry and exit route for atmospheric air. The difference between atmospheric pressure and the pressure in the measuring cell is strongly linearly correlated with the pump flowrate and suggests that the air flux through the chamber is controlled by the membrane pump. In spite of the air flux we find it does not affect the determination of soil CO_2 fluxes, but does complicate assessment of F_G and $X_{CO_2,G}$.

A method to compute both the CO_2 molar fraction of soil gas and the flux of the soil gas mixture from CO_2 time series is presented. The data are useful to provide a better understanding of the gas flux in natural systems

and are needed for studies when chamber gas is collected for ^{13}C-CO_2 analyses.

REFERENCES

Allard P., Carbonnelle J., Dajlevic D., Le Bronec J., Morel P., Robe M.C., Maurenas J.M., Faivre-Pierret R., Martin D., Sabroux J.C., Zettwoog P. (1991). Eruptive and diffuse emissions of CO_2 from Mount Etna. Nature, 351, 387-391.

Baubron J.C., Allard P., Toutain J.P. (1990). Diffuse volcanic emissions of carbon dioxide from Vulcano Island, Italy. Nature, 344, 51-53.

Baubron J.C., Allard P., Sabroux J.C., Tedesco D., Toutain, J.P. (1991). Soil gas emanations as precursory indicators of volcanic eruptions. J. Geol. Soc. London, 148, 571-576.

Bergfeld D., Goff F., Janik C.J. (2001). Elevated carbon dioxide flux at the Dixie Valley geothermal field, Nevada; relations between surface phenomena and the geothermal reservoir. Chem. Geol., 177, 43-66.

Brombach T., Hunziker J.C., Chiodini G., Cardellini C., Marini L. (2001). Soil diffuse degassing and thermal energy fluxes from the southern Lakki plain, Nisyros (Greece). Geophys. Res. Lett., 28, 69-72.

Brusca L., Inguaggiato S., Longo M., Madonia P., Maugeri R. (2004). The 2002–2003 eruption of Stromboli (Italy): Evaluation of the volcanic activity by means of continuous monitoring of soil temperature, CO_2 flux, and meteorological parameters. Geochem. Geophys. Geosyst., 5, Q12001, doi:10.1029/2004GC000732.

Carapezza M.L., Federico C. (2000). The contribution of fluid geochemistry to the volcano monitoring of Stromboli. J. Volcanol. Geotherm. Res., 95, 227-245.

Carapezza M.L., Granieri D. (2004). CO_2 soil flux at Vulcano (Italy): comparison between active and passive methods. Appl. Geochem., 19, 73-88.

Carapezza M.L., Ricci T., Ranaldi M., Tarchini L. (2009). Active degassing structures of Stromboli and variations in diffuse CO_2 output related to the volcanic activity. J. Volcanol. Geotherm. Res., 182, 231-245.

Chiodini G., Frondini F., Raco B. (1996) Diffuse emission of CO_2 from the Fossa crater, Vulcano Island (Italy). Bull. Volcanol., 58, 41-50.

Chiodini G., Cioni R., Guidi M., Raco B., Marini L. (1998). Soil CO_2 flux measurements in volcanic and geothermal areas. Appl. Geochem., 13, 543-552.

Chiodini G., Frondini F., Cardellini C., Granieri D., Marini

L., Ventura G. (2001). CO$_2$ degassing and energy release at Solfatara volcano, Campi Flegrei, Italy. J. Geophys. Res., 106(B8), 16213-16221.

Chiodini G., Baldini A., Barberi F., Carapezza M.L., Cardellini C., Frondini F., Granieri D., Ranaldi M. (2007). Carbon dioxide degassing at Latera caldera (Italy): evidence of geothermal reservoir and evaluation of its potential energy. J. Geophys. Res., 112, B12204, doi:10.1029/2006JB004896.

Chiodini G., Caliro S., Cardellini C., Avino R., Granieri D., Schmidt A. (2008). Carbon isotopic composition of soil CO$_2$ efflux, a powerful method to discriminate different sources feeding soil CO$_2$ degassing in volcanic-hydrothermal areas. Earth Planet. Sci. Lett., 274, 372-379.

Dionis S.M., Melián G., Rodríguez F., Hernández P.A., Padrón E., Pérez N.M., Barrancos J., Padilla G.ermán, Sumino H., Fernandes P., Bandomo Z., Silva S., Pereira J.M., Semedo H. (2015). Diffuse volcanic gas emission and thermal energy release from the summit crater of Pico do Fogo, Cape Verde. Bull. Volcanol., 77, 1-13.

Edwards N.T. (1975). Effects of temperature and moisture on carbon dioxide evolution in a mixed deciduous forest floor. Soil Sci. Soc. Am. Proc., 39, 361–365.

Evans W.C., Sorey M.L., Kennedy B.M., Stonestrom D.A., Rogie J.D., Shuster D.L. (2001). High CO$_2$ emissions through porous media: Transport mechanisms and implications for flux measurement and fractionation, Chem. Geol., 177, 15 – 29.

Evans W.C., Bergfeld D., McGimsey R.G., Hunt A.G. (2009). Diffuse gas emissions at the Ukinrek Maars, Alaska: Implications for magmatic degassing and volcanic monitoring. Appl. Geochem., 24, 527-535.

Faure G. (1986). Principles of isotope geology. 2nd edition. Wiley, New York, 589 pp.

Federico C., Corso P.P., Fiordilino E., Cardellini C., Chiodini G., Parello F., Pisciotta A. (2010). CO$_2$ degassing at La Solfatara volcano (Phlegrean Fields): Processes affecting δ13C and δ18O of soil CO$_2$. Geochim. Cosmochim. Acta, 74, 3521-3538.

Fridriksson T., Kristjánsson B.R., Ármannsson H., Margrétardóttir E., Ólafsdóttir S., Chiodini G. (2006). CO$_2$ emissions and heat flow through soil, fumaroles, and steam heated mud pools at the Reykjanes geothermal area, SW Iceland. Appl. Geochem., 21, 1551-1569.

Frondini F., Chiodini G., Caliro S., Cardellini C., Granieri D., Ventura G. (2004). Diffuse CO$_2$ degassing at Vesuvio, Italy. Bull. Volcanol., 66, 642–651.

Frondini F., Caliro S., Cardellini C., Chiodini G., Morgantini N. (2009). Carbon dioxide degassing and ther-

mal energy release in the Monte Amiata volcanic-geothermal area (Italy). Appl. Geochem., 24, 860-875.

Gerlach T., Doukas M., McGee K., Kessler R. (2001). Soil efflux and total emission rates of magmatic CO$_2$ at the Horseshoe Lake tree kill, Mammoth Mountain, California. Chem. Geol., 177, 101–116.

Granieri, D., Chiodini, G., Marzocchi, W., Avino, R. (2003). Continuous monitoring of CO$_2$ soil diffuse degassing at Phlegraean Fields (Italy): influence of environmental and volcanic parameters. Earth Plan. Sci. Lett. 212, 167–179.

Granieri D., Avino R., Chiodini G. (2010) Carbon dioxide diffuse emission from the soil: ten years of observations at Vesuvio and Campi Flegrei (Pozzuoli), and linkages with volcanic activity. Bull. Volcanol., 72, 103–118.

Hanson P.J., Wullschleger S.D., Bohlman S.A., Todd D.E. (1993). Seasonal and topographic patterns of forest floor CO$_2$ efflux from an upland oak forest. Tree Physiol., 13, 1-15.

Healy R.W., Striegl R.G., Russell T.F., Hutchinson G.L., Livingston G.P. (1996). Numerical evaluation of static-chamber measurements of soil-atmosphere gas exchange: identification of physical processes. Soil Sci. Soc. Am. J., 60, 740-747.

Hernández P.A., Pérez N.M., Salazar J.M., Nakai S., Notsu K., Wakita H. (1998). Diffuse emissions of carbon dioxide, methane, and hellium-3 from Teide volcano, Tenerife, Canary Islands, Geophys. Res. Lett., 25, 3311–3314, doi:10.1029/98GL02561.

Hernández P.A., Salazar J.M., Shimoike Y., Mori T., Notsu K., Pérez N. (2001). Diffuse emission of CO$_2$ from Miyakejima volcano, Japan. Chem. Geol., 177, 175-185.

Hutchison W., Mather T.A., Pyle D.M., Biggs J., Yirgu G. (2015). Structural controls on fluid pathways in an active rift system: a case study of the Aluto volcanic complex. Geosphere 11, 542–562.

Hutchison W., Biggs J., Mather T.A., Pyle D.M., Lewi E., Yirgu G., Caliro S., Chiodini G., Clor L.E., Fischer T.P. (2016). Causes of unrest at silicic calderas in the East African Rift: New constraints from InSAR and soil-gas chemistry at Aluto volcano, Ethiopia. Geochem. Geophys. Geosyst., 17, 3008– 3030, doi:10.1002/2016GC006395.

Jolie E., Klinkmueller M., Moeck I. (2015). Diffuse surface emanations as indicator of structural permeability in fault-controlled geothermal systems. J. Volcanol. Geotherm. Res., 290, 97-113.

Lee H., Muirhead J.D., Fischer T.P., Ebinger C.J., Kattenhorn S.A., Sharp Z.D., Kianji G. (2016). Massive and

prolonged deep carbon emissions associated with continental rifting. Nature Geoscience. DOI: 10.1038/NGEO2622.

Leib T.M., Pereira C.J. (2008). Reaction Kinetics Section 7. In: Perry's Chemical Engineers' Handbook 8th edition.

Lewicki J.L. Brantley S.L. (2000). CO_2 degassing along the San Andreas fault, Parkfield, California. Geophys. Res. Lett. 27, 5–8.

Lewicki J.L., Hilley G.E. (2014). Multi-scale observations of the variability of magmatic CO_2 emissions, Mammoth Mountain, CA, USA. J. Volcanol. Geotherm. Res., 284, 1-15.

Lewicki J.L., Bergfeld D., Cardellini C., Chiodini G., Granieri D., Varley N., Werner C. (2005). Comparative soil CO_2 flux measurements and geostatistical estimation methods on Masaya volcano, Nicaragua. Bull. Volcanol., 68, 76-90.

Lewicki J.L., Hilley G.E., Tosha T., Aoyagi R., Yamamoto K., Benson S.M. (2007). Dynamic coupling of volcanic CO_2 flow and wind at the Horseshoe Lake tree kill, Mammoth Mountain, California. Geophys. Res. Lett., 34, L03401, doi:10.1029/2006GL028848.

Mazot A., Rouwet D., Taran Y., Inguaggiato S., Varley N. (2011). CO_2 and He degassing at El Chichón volcano, Chiapas, Mexico: gas flux, origin and relationship with local and regional tectonics. Bull. Volcanol., 73, 423-441.

Norman J.M., Garcia R., Verma S.B. (1992). Soil surface CO_2 fluxes and the carbon budget of a grassland. J. Geophys. Res., 97, 18845-18853.

Norman J.M., Kucharik C.J., Gower S.T., Baldocchi D.D., Crill P.M., Rayment M., Savage K., Strieglfi R.G. (1997). A comparison of six methods for measuring soil-surface carbon dioxide fluxes. J. Geophys. Res.,102, 28-771.

Notsu K., Sugiyama K., Hosoe M., Uemura A., Shimoike Y., Tsunomori F., Sumino H., Yamamoto J., Mori T., Hernández P.A. (2005). Diffuse CO_2 efflux from Iwojima volcano, Izu-Ogasawara arc, Japan. J. Volcanol. Geotherm. Res.,139, 147-161.

Padilla G.D., Hernández P.A., Pérez N.M., Pereda E., Padrón E., Melián G., Herrera M. (2014). Anomalous diffuse CO_2 emissions at the Masaya Volcano (Nicaragua) related to seismic-volcanic unrest. Pure and Appl. Geophys., 171, 1791-1804.

Padrón E., Hernández P.A., Toulkeridis T., Pérez N.M., Marrero R., Melián G., Virgili G., Notsu K. (2008a). Diffuse CO_2 emission rate from Pululahua and the lake-filled Cuicocha calderas, Ecuador. J. Volcanol. Geotherm. Res., 176, 163-169.

Padrón E., Melián G., Marrero R., Nolasco D., Barrancos J.,

Padilla G., Hernández P.A., Pérez N.M. (2008b). Changes in the diffuse CO_2 emission and relation to seismic activity in and around El Hierro, Canary Islands, Pure Appl. Geophys., 165, 95–114, doi:10.1007/s00024-007-0281-9.

Parks M.M., Caliro S., Chiodini G., Pyle D.M., Mather T.A., Berlo K., Edmonds M., Biggs J., Nomikou P., Raptakis C. (2013). Distinguishing contributions to diffuse CO_2 emissions in volcanic areas from magmatic degassing and thermal decarbonation using soil gas 222Rn–δ13C systematics: Application to Santorini volcano, Greece. Earth Planet. Sci. Lett., 377, 180-190.

Pérez N.M., Padilla G.D., Padrón E., Hernández P.A., Melián G.V., Barrancos J., Dionis S., Nolasco D., Rodríguez F., Calvo D., Hernández Í. (2012) Precursory diffuse CO_2 and H2S emission signatures of the 2011–2012 El Hierro submarine eruption, Canary Islands. Geophys. Res. Lett., 39, L16311, doi:10.1029/2012GL052410.

Rinaldi A.P., Vandemeulebrouck J., Todesco M., Viveiros F. (2012). Effects of atmospheric conditions on surface diffuse degassing, J. Geophys. Res., 117, B11201, doi:10.1029/2012JB009490.

Rissmann C., Christenson B., Werner C., Leybourne M., Cole J., Gravley D. (2012). Surface heat flow and CO_2 emissions within the Ohaaki hydrothermal field, Taupo Volcanic Zone, New Zealand. Appl. Geochem., 27, 223-239.

Rogie J.D., Kerrick D.M., Sorey M.L., Chiodini G., Galloway D.L. (2001). Dynamics of carbon dioxide emission at Mammoth Mountain, California. Earth Planet. Sci. Lett., 188, 535-541.

Robertson E., Biggs J., Edmonds M., Clor L., Fischer T.P., Vye-Brown C., Kianji G., Koros W., Kandie R. (2016). Diffuse degassing at Longonot volcano, Kenya: Implications for CO_2 flux in continental rifts. J. Volcanol. Geotherm. Res. http://dx.doi.org/10.1016/j.jvolgeores.2016.06.016 (in press).

Salazar J.M., Hernández P.A., Pérez N.M., Melián G., Álvarez J., Segura F., Notsu K. (2001). Diffuse emission of carbon dioxide from Cerro Negro volcano, Nicaragua, Central America. Geophys. Res. Lett., 28, 4275-4278.

Salazar J.M.L., Pérez N.M., Hernández P.A., Soriano T., Barahona F., Olmos R., Cartagena R. , López D.L., Lima R.N., Melián G., Galindo I., Padrón E., Sumino H., Notsu K. (2002) Precursory diffuse carbon dioxide degassing signature related to a 5.1 magnitude earthquake in El Salvador, Central America. Earth Planet. Sci. Lett., 205, 81-89.

Toutain J.P., Sortino F., Baubron J.C., Richon P., Sumarti S., Nonell A. (2009). Structure and CO$_2$ budget of Merapi volcano during inter-eruptive periods. Bull. Volcanol., 71, 815-826.

Viveiros F., Ferreira T., Vieira J.C., Silva C., Gaspar, J.L. (2008). Environmental influences on soil CO$_2$ degassing at Furnas and Fogo volcanoes (São Miguel Island, Azores archipelago). J. Volcanol. Geotherm. Res., 177, 883-893.

Viveiros F., Ferreira T., Silva C., Gaspar J.L. (2009). Meteorological factors controlling soil gases and indoor CO$_2$ concentration: a permanent risk in degassing areas. Sci. Total Environ., 407, 1362–1372.

Viveiros F., Cardellini C., Ferreira T., Caliro S., Chiodini G., Silva C. (2010). Soil CO$_2$ emissions at Furnas volcano, São Miguel Island, Azores archipelago: Volcano monitoring perspectives, geomorphologic studies, and land use planning application. J. Geophys. Res., 115, B12208, doi:10.1029/2010JB007555.

Welles J.M., Demetriades-Shah T.H., McDermitt D.K. (2001). Considerations for measuring ground CO$_2$ effluxes with chambers. Chem. Geol., 177, 3-13.

Werner C., Cardellini C. (2006). Comparison of carbon dioxide emissions with fluid upflow, chemistry, and geologic structures at the Rotorua geothermal system, New Zealand. Geothermics, 35, 221-238.

Werner C., Brantley S.L., Boomer K. (2000) CO$_2$ emissions related to the Yellowstone volcanic system 2. Statistical sampling, total degassing, and transport mechanisms. J. Geophys. Res., 105, B5, 10,831-10,846.

Werner C., Bergfeld D., Farrar C.D., Doukas M.P., Kelly P.J., Kern C. (2014). Decadal-scale variability of diffuse CO$_2$ emissions and seismicity revealed from long-term monitoring (1995–2013) at Mammoth Mountain, California, USA. J. Volcanol. Geotherm. Res., 289, 51-63.

Xu L., Furtaw M.D., Madsen R.A., Garcia R.L., Anderson D.J., McDermitt D.K. (2006). On maintaining pressure equilibrium between a soil CO$_2$ flux chamber and the ambient air. J. Geophys. Res., 111, D08S10, doi:10.1029/2005JD006435.

Ana Hernández-Rodríguez

*CORRESPONDING AUTHOR: Ana Hernández-RODRÍGUEZ,

West Systems s.r.l., Florence

Italy

email: ana.hernandezrodriguez@unifi.it